



## Optical microprism cavities based on dislocation-free GaN

Downloaded from: <https://research.chalmers.se>, 2026-03-10 06:56 UTC

Citation for the original published paper (version of record):

Hjort, F., Khalilian, M., Bengtsson, J. et al (2020). Optical microprism cavities based on dislocation-free GaN. *Applied Physics Letters*, 117(23). <http://dx.doi.org/10.1063/5.0032967>

N.B. When citing this work, cite the original published paper.

# Optical microprism cavities based on dislocation-free GaN

Cite as: Appl. Phys. Lett. **117**, 231107 (2020); <https://doi.org/10.1063/5.0032967>

Submitted: 12 October 2020 . Accepted: 28 November 2020 . Published Online: 09 December 2020

 Filip Hjort, Maryam Khalilian, Jörgen Bengtsson, Marcus Bengths, Johan Gustavsson,  Anders Gustafsson, Lars Samuelson, and  Åsa Haglund



View Online



Export Citation



CrossMark

## ARTICLES YOU MAY BE INTERESTED IN

[Defect-related photoluminescence and photoluminescence excitation as a method to study the excitonic bandgap of AlN epitaxial layers: Experimental and ab initio analysis](#)

Applied Physics Letters **117**, 232101 (2020); <https://doi.org/10.1063/5.0027743>

[Band alignment of ScAlN/GaN heterojunction](#)

Applied Physics Letters **117**, 231105 (2020); <https://doi.org/10.1063/5.0029488>

[Carrier dynamics near a crack in GaN microwires with AlGaIn multiple quantum wells](#)

Applied Physics Letters **117**, 221105 (2020); <https://doi.org/10.1063/5.0023545>



## Your Qubits. Measured.

Meet the next generation of quantum analyzers

- Readout for up to 64 qubits
- Operation at up to 8.5 GHz, mixer-calibration-free
- Signal optimization with minimal latency

Find out more



# Optical microprism cavities based on dislocation-free GaN

Cite as: Appl. Phys. Lett. **117**, 231107 (2020); doi: [10.1063/5.0032967](https://doi.org/10.1063/5.0032967)

Submitted: 12 October 2020 · Accepted: 28 November 2020 ·

Published Online: 9 December 2020



View Online



Export Citation



CrossMark

Filip Hjort,<sup>1,a)</sup>  Maryam Khalilian,<sup>2</sup> Jörgen Bengtsson,<sup>1</sup> Marcus Bengths,<sup>1</sup> Johan Gustavsson,<sup>1</sup> Anders Gustafsson,<sup>2</sup>  Lars Samuelson,<sup>2</sup> and Åsa Haglund<sup>1</sup> 

## AFFILIATIONS

<sup>1</sup>Department of Microtechnology and Nanoscience, Chalmers University of Technology, 412 96 Gothenburg, Sweden

<sup>2</sup>Solid State Physics and NanoLund, Lund University, 221 00 Lund, Sweden

<sup>a)</sup> Author to whom correspondence should be addressed: [filip.hjort@chalmers.se](mailto:filip.hjort@chalmers.se)

## ABSTRACT

Three-dimensional growth of nanostructures can be used to reduce the threading dislocation density that degrades III-nitride laser performance. Here, nanowire-based hexagonal GaN microprisms with flat top and bottom c-facets are embedded between two dielectric distributed Bragg reflectors to create dislocation-free vertical optical cavities. The cavities are electron beam pumped, and the quality ( $Q$ ) factor is deduced from the cavity-filtered yellow luminescence. The  $Q$  factor is  $\sim 500$  for a 1000 nm wide prism cavity and only  $\sim 60$  for a 600 nm wide cavity, showing the strong decrease in  $Q$  factor when diffraction losses become dominant. Measured  $Q$  factors are in good agreement with those obtained from quasi-3D finite element frequency-domain method and 3D beam propagation method simulations. Simulations further predict that a prism cavity with a 1000 nm width will have a  $Q$  factor of around 2000 in the blue spectral regime, which would be the target regime for real devices. These results demonstrate the potential of GaN prisms as a scalable platform for realizing small footprint lasers with low threshold currents.

© 2020 Author(s). All article content, except where otherwise noted, is licensed under a Creative Commons Attribution (CC BY) license (<http://creativecommons.org/licenses/by/4.0/>). <https://doi.org/10.1063/5.0032967>

The III-nitrides are an essential materials system used for both optical and electrical devices, including LEDs, high-electron-mobility transistors (HEMTs), and lasers.<sup>1–3</sup> The performance of these devices is strongly dependent on material quality. III-nitrides suffer from much higher threading dislocation densities than most other materials systems,<sup>4</sup> and even though dislocations are less detrimental to III-nitrides than to other semiconductors,<sup>4</sup> high dislocation densities can, for example, lead to an increased non-radiative recombination rate in quantum wells (QWs)<sup>5</sup> and larger leakage currents in HEMTs.<sup>6</sup> For lasers, dislocations reduce the device lifetime, and commercial GaN-based lasers are therefore grown on free-standing GaN substrates with a dislocation density of approximately  $10^6 \text{ cm}^{-2}$  or below.<sup>3,7</sup> This is also true for state-of-the-art blue-emitting GaN-based vertical-cavity surface-emitting lasers (VCSELs).<sup>8,9</sup> Unfortunately, free-standing GaN substrates are limited in size and significantly more expensive than GaN templates on sapphire, which despite their high dislocation densities of  $\sim 10^7\text{--}10^8 \text{ cm}^{-2}$  are the standard substrates for commercial LEDs.

Three-dimensional growth of nanowires (NWs) is a method that can prevent threading dislocations from propagating from the

substrate into device layers.<sup>10,11</sup> NWs and other nanostructures also have additional benefits such as small footprint and that they allow for incorporation of higher strain during growth.<sup>12–14</sup> Furthermore, the miniaturized size supports fabrication of lasers with low threshold currents. These and other benefits have led to intense research on III-nitride nanostructure lasers,<sup>15–25</sup> including demonstrations of optically pumped vertical cavities.<sup>20–25</sup> However, the vertical cavity lasers have mainly been formed using a top-down fabrication process<sup>20</sup> or have used optical pumping of the entire III-nitride cavity,<sup>21–23</sup> or both.<sup>24,25</sup> Top-down fabrication may result in etch-induced damages and does not benefit from any dislocation filtering, while the modal gain reached when optically pumping the entire cavity is higher than would be achievable in devices where only the QWs supply optical gain. Thus, there is still a need to realize dislocation-free vertical cavities that can support lasing from a QW gain region, i.e., a structure suitable for use in future electrically injected devices.

Although three-dimensional growth of GaN nanowires is useful to reduce threading dislocations, it normally results in structures with pyramid-shaped tips<sup>10,11,26</sup> that are unsuitable for use in vertical cavities. We recently demonstrated the growth of dislocation-free and

micrometer-sized hexagonal GaN prisms that instead of pyramidal tips have atomically flat top *c*-facets, achieved by an *in situ* reformation step.<sup>27</sup> In this paper, we demonstrate the potential of these dislocation-free hexagonal prisms to form the central building block of vertical microcavity lasers. This demonstration is achieved by embedding the prisms in dielectric distributed Bragg reflectors (DBRs) and investigating the dependence of the quality (*Q*) factor on the width of the prism, both through cathodoluminescence (CL) measurements and simulations. In this way, we show that GaN prisms have a sufficiently high *Q* factor to be a viable option for producing small footprint and long lifetime VCSELs grown on low-cost GaN templates.

The GaN prisms were grown by metalorganic chemical vapor deposition (MOCVD) based on the selective area epitaxy of GaN. The growth is described in detail in Ref. 27 and in the [supplementary material](#). Figure 1(a) shows scanning electron microscope (SEM) images of a GaN prism array where the homogeneous symmetric shapes are evidence of the complete absence of dislocations in the structures.<sup>27</sup>

To evaluate the potential of the GaN prisms for high-quality optical microcavities, cavities were fabricated by sandwiching single prisms between two dielectric HfO<sub>2</sub>/SiO<sub>2</sub> DBRs, as shown

schematically in Fig. 1. Prisms with a width of  $w_{\text{prism}} \approx 1000$  nm (in the following defined as the long diagonal of the hexagonal cross section) and 600 nm were transferred onto a planar 11.5 pair DBR on silicon using an OmniProbe manipulator in an SEM. By pushing the GaN prism on the side with the manipulator, the prism was detached from the substrate and attached to the probe, as shown in Figs. 1(b) and 1(c). The attached prism was then placed on the first mirror and bonded to it by van der Waals forces, as shown in Fig. 1(d). Finally, a top 10 pair DBR was deposited over the entire sample so that the DBR wraps around the prism as seen schematically in Figs. 1(e) and 1(f). Figure 1(g) shows a cross-sectional scanning transmission electron microscopy (STEM) image of an approximately 100 nm thick lamella, thinned down using a focused ion beam, of a prism with a top DBR but standing on top of a Si substrate instead of a bottom DBR, and where it is clearly visible how the DBR wraps around the prism. The DBRs were fabricated by reactive sputtering using an FHR MS150 magnetron sputter. For HfO<sub>2</sub>, the radio frequency power was 0.75 kW, the pressure was  $1.4 \times 10^{-2}$  mbar, the Ar flow was 80 sccm, and the O<sub>2</sub> flow was 6 sccm. The corresponding parameters for SiO<sub>2</sub> were 1 kW,  $1.3 \times 10^{-2}$  mbar, 40 sccm, and 15 sccm.

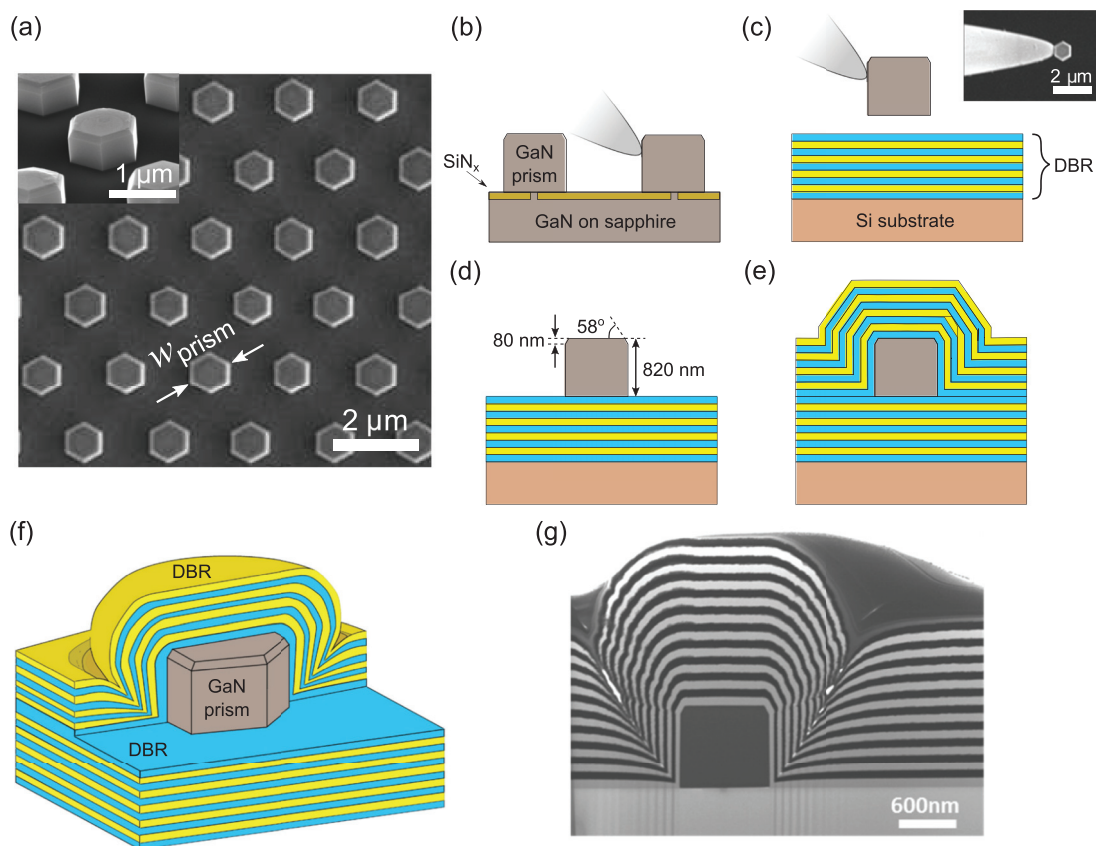


**FIG. 1.** (a) Top-view SEM image of an as-grown array of GaN microprisms. The inset shows a tilted-view SEM image of a single prism. (b)–(e) Cross-sectional schematic of the microcavity fabrication. The as-grown prism is (b) detached and (c) transferred using a micro-manipulator, followed by (d) placement on top of an 11.5 pair HfO<sub>2</sub>/SiO<sub>2</sub> DBR on Si. (e) The cavity is finalized by depositing a 10 pair HfO<sub>2</sub>/SiO<sub>2</sub> DBR. (f) Three-dimensional schematic of the vertical microcavity and (g) STEM image of a prism placed directly on a Si substrate without the bottom DBR but after top DBR deposition.

To measure the  $Q$  factor of a single optical microcavity, CL was used to locally induce and detect yellow luminescence (YL), commonly observed from point defects in GaN.<sup>28</sup> The YL acts as a localized light source, which allows us to probe the intrinsic structural  $Q$  factor of a single microcavity as the YL, unlike the bandgap emission, is not associated with any significant material absorption.<sup>28</sup> Both DBRs were designed to have a stop band center wavelength at the YL band, i.e., at 550 nm, corresponding to 67.1 nm thick  $\text{HfO}_2$  layers and 94.0 nm thick  $\text{SiO}_2$  layers. The measured reflectivity at the design wavelength for the bottom DBR was 99.5%, and the 85 nm wide stop band (>99%) covers the YL.

CL was used to probe three different structures: as-grown prisms (i.e., without DBRs), prism microcavities, and the top DBR resting directly on the bottom DBR without any prism in between. The CL was performed at room temperature in a dedicated SEM equipped with a hyperspectral detection system using a CCD to detect the emission with both spectral and spatial resolution. The measurements were performed at 30 keV, with a probe current of 200–500 pA and a spectral resolution of about 0.5 nm. The high acceleration voltage ensured significant excitation of the prism through the top mirror.

To confirm the results from the CL measurements and to predict the performance of some future realization of optical cavities, numerical electromagnetic field simulations of microprism cavities with different prism widths were performed. As all numerical methods involve approximations, two methods, whose approximations differ, were used. First, quasi-3D circularly symmetric simulations using the finite element frequency domain method (Q3D-FEM) were performed using COMSOL Multiphysics. The hexagonal cross section of the prism was approximated with a circle of equal area, so that the equivalent diameter of the circular cross section was 940 nm for a hexagon long diagonal length of 1030 nm, which was assumed as the diagonal

length for the large  $w_{\text{prism}} \approx 1000$  nm prisms. The equal area approximation has been shown to be accurate for waveguiding and facet reflection behavior for light propagation in the vertical direction in the case of nanowires.<sup>29</sup> Second, a fully 3D scalar beam propagation method (3D-BPM) was implemented in MATLAB to simulate a structure identical to the one used for the Q3D-FEM. The only difference was that the true hexagonal cross section of the prism cavity was used instead of the approximated circle of equal area, and that the tilted s-planes were approximated by staircase structures. More details on the two simulation methods can be found in the [supplementary material](#).

Figure 2(a) shows the spectra of the YL from an as-grown prism, a prism with a width of approximately 1000 nm between two DBRs, as well as the CL emission from the mirrors themselves as this structure emits light when pumped by the electron beam. The region with low intensity in the DBR only spectrum is an indication of the width of the DBR stop band. The measured full width at half maximum (FWHM) of the prism cavity resonance peak at 550 nm is approximately 1 nm, which yields a  $Q$  factor of  $Q_{\text{prism}} \approx \lambda_{\text{res}}/\Delta\lambda_{\text{res}} \approx 500$ . A number of prism cavities with similar widths were evaluated and they all showed  $Q$  factors between 410 and 580 (see [Table I](#)). The CL spectra of the prism cavities show two distinct resonance peaks, one sharp at a shorter wavelength and one broader resonance at a longer wavelength, as seen in [Fig. 2\(b\)](#). The two peaks correspond to two different longitudinal modes as confirmed by simulations using the Q3D-FEM mode solver, yielding solutions with similar spectral spacing ( $\sim 10\%$  larger than measured).

The variation in the different prism cavities' resonance wavelengths can be explained by a high sensitivity of the resonance wavelengths to the exact height of the prism. Nevertheless, the yellow luminescence band is spectrally broad enough to act as a broadband light source, making this excitation method insensitive to the height variations. Simulations of prism cavities with different total heights in

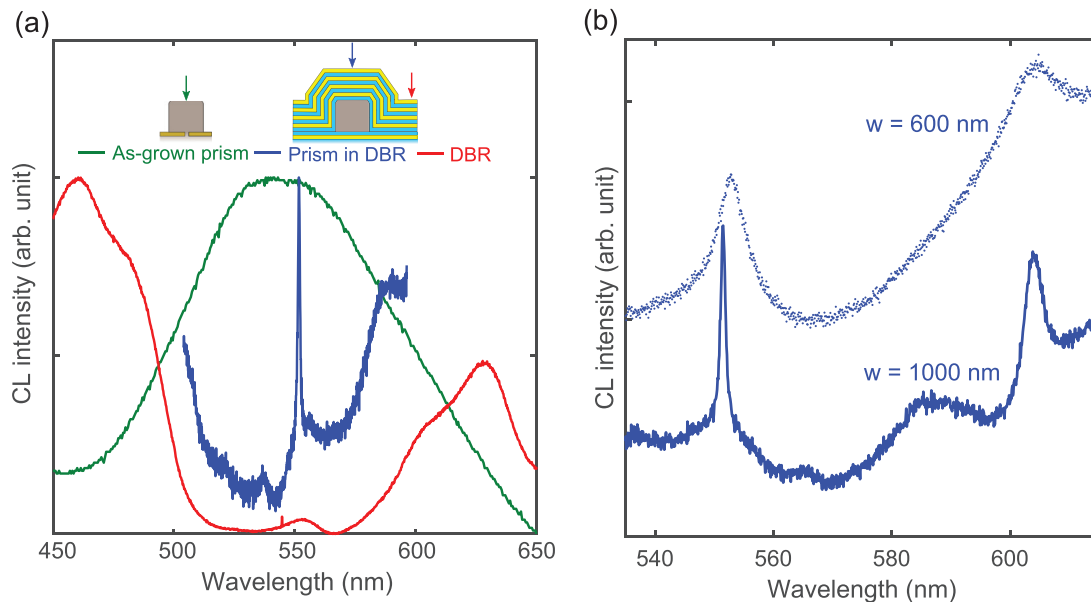


**FIG. 2.** (a) Emission spectra from an as-grown prism, showing the non-resonant YL (green), from a single prism embedded between two DBRs (blue), showing one narrow longitudinal resonance, and from a position where the top DBR rests directly on the bottom DBR (red). (b) Emission spectra from a larger-width (solid) and smaller-width (dotted) prism embedded between two DBRs.

**TABLE I.** Measured resonance wavelengths for two optical resonances (labeled 1 and 2), FWHM of the resonance peaks, and corresponding Q factors for six prism cavities with a long diagonal width of  $w_{\text{prism}} \approx 1000$  nm.

Prism cavity #	Peak 1 (nm)	FWHM 1 (nm)	Q factor 1	Peak 2 (nm)	FWHM 2 (nm)	Q factor 2
1	516	0.9	573	563	1.6	352
2	523	0.9	581	577	1.5	385
3	534	1.1	485	588	2.4	245
4	535	1.3	412	589	3.6	164
5	543	1	543	597	2.8	213
6	551	1.1	501	604	3.3	183

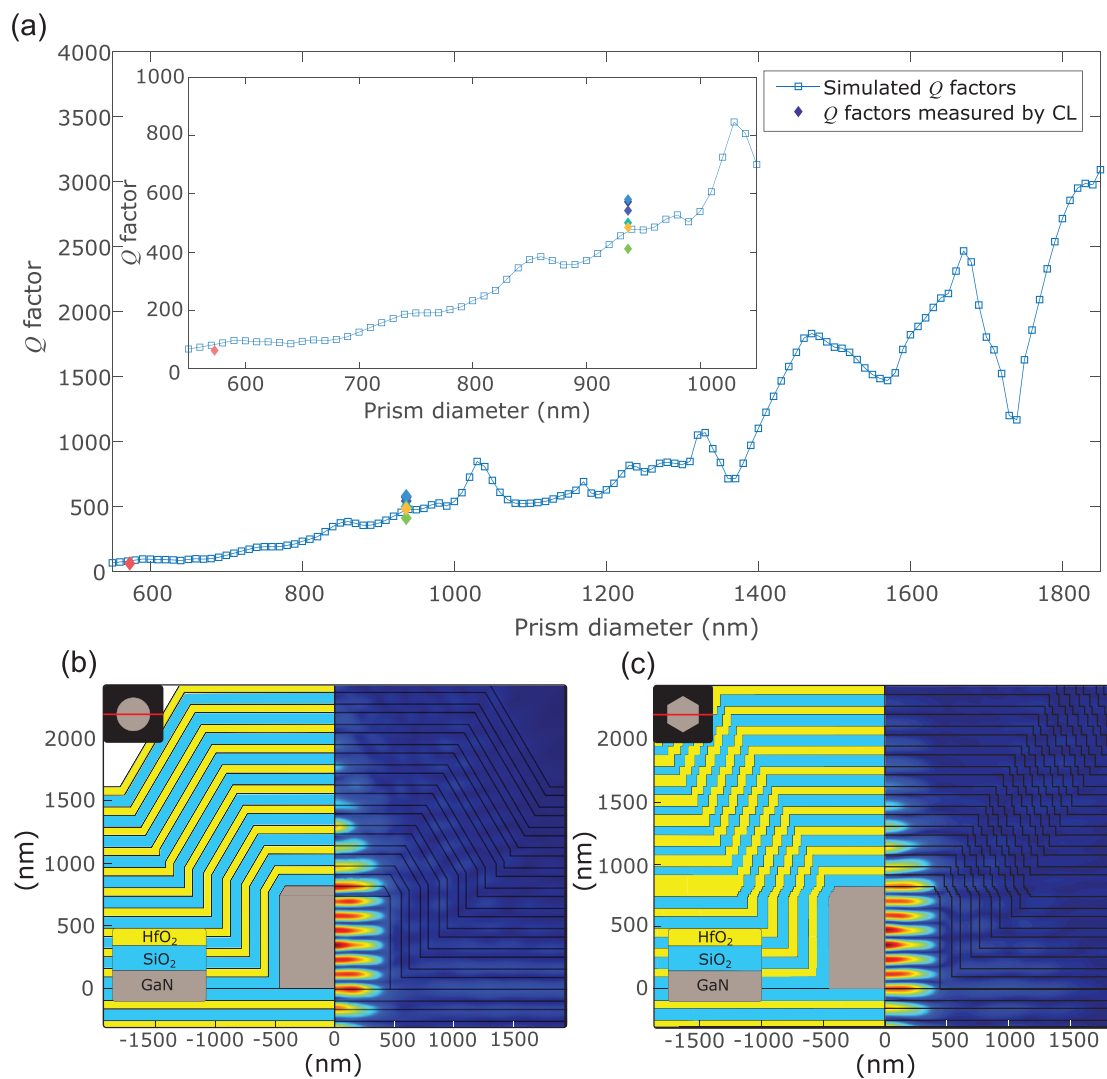


**FIG. 3.** Prism cavity Q factors obtained from CL measurements (diamonds) and Q3D-FEM simulations (connected squares) for a GaN-prism cavity with different diameters. The inset is a magnification of the small-diameter region. (b) and (c) Geometry (left half of figure) and magnitude of the optical field in linear scale (right half) for a prism simulated using (b) Q3D-FEM with a circularly symmetric geometry (940 nm diameter) and (c) 3D-BPM with a hexagonal geometry (890 nm short diagonal, 1030 nm long diagonal). The red line in the inset in (b) and (c) marks the top-view direction of the cross section.

the range of 750–820 nm showed that the  $Q$  factor of the resonance in the spectral range of 516–551 nm is relatively independent of the wavelength, as confirmed by the CL data in Table I. The longitudinal resonance with the shorter resonance wavelength, labeled Peak 1 in Table I, always has a smaller FWHM, and thereby a higher  $Q$  factor, than the longer resonance wavelength. This is seen in measurements as well as in the simulations using both the Q3D-FEM and a 3D-BPM method and is caused by the larger relative optical size of the prism for shorter wavelengths and thus lower diffractive losses. Figure 2(b) also shows the emission spectrum from a GaN-prism cavity with a smaller width,  $w_{\text{prism}} \approx 600$  nm. The  $Q$  factor of the smaller-sized prism cavity is as low as  $Q_{\text{prism}} \approx 60$ , indicating a strong dependence of the  $Q$  factor on the width of the prism. Furthermore, CL measurements on a cavity formed from a GaN prism lying on its side did not show any resonance peaks, verifying that the geometry is essential for the cavity formation.

To confirm the strong dependence of the  $Q$  factor on the geometry of the prism cavity, the measured  $Q$  values are compared with those obtained from simulations. Figure 3(a) shows the results of the simulations using the Q3D-FEM mode solver. As expected, the trend is clearly that the  $Q$  factor increases with the prism width. This is because scattering and diffraction loss for the resonant optical field generally decrease with a larger width, leading to a reduced cavity loss and, therefore, a higher  $Q$  factor. The simulated  $Q$  factors agree well with the measured. The same trend was observed using the 3D-BPM method, although simulations were done for much fewer prism widths because of the long computation time compared with Q3D-FEM. Figure 3(b) presents a Q3D-FEM simulated electric field profile in cross section along with the assumed geometry and in Fig. 3(c) the corresponding cross sections are seen for 3D-BPM. Both show similar standing wave patterns in the vertical cavity. With 3D-BPM, the extracted  $Q$  factors were higher by roughly a factor of two, which is not remarkable considering the high sensitivity of the  $Q$  factor to the detailed structure of the microcavity. The high sensitivity can be directly appreciated from Fig. 3(a), which shows that irregular and significant oscillations may occur in the  $Q$  factor as the prism diameter changes slightly. This oscillatory behavior has been investigated for circularly symmetric AlGaAs micropillars and was then attributed to

changes in coupling between different Bloch modes in the structure.<sup>30,31</sup>

To achieve lasing in GaN-based blue VCSELs at room temperature,  $Q$  factors of  $\sim 500$  have proven to be sufficient.<sup>32</sup> The prism resonators demonstrated here, with measured  $Q_{\text{prism}} \approx 500$  at a 550 nm wavelength, may, thus, be of sufficiently high optical quality to be used for microlasers. Furthermore, at the target wavelength for a GaN-prism VCSEL, which would be in the blue spectral regime, the  $Q$  factor is expected to be substantially higher for a prism cavity of the same physical size. This is due to the size of the prism being larger in relation to the wavelength, which results in lower scattering and diffraction losses and thereby higher  $Q$  factors. To quantify this effect, the  $Q$  factor vs prism diameter was simulated with Q3D-FEM for a prism cavity identical to the prism cavity simulated at 550 nm but with refractive indices valid for a wavelength of 420 nm and DBRs designed for 420 nm (thicknesses of the DBR layers of 49.8 nm for  $\text{HfO}_2$  and 71.3 nm for  $\text{SiO}_2$ ). The results are shown in Fig. 4. For the same diameter of the prism, there is about a fourfold increase in the  $Q$  factor for the 420-nm wavelength cavity compared with that of the 550-nm cavity. One of the first demonstrations of a continuous-wave electrically injected GaN-based blue VCSEL used a cavity with a reported  $Q$  factor of 1800.<sup>33</sup> Even though electrically pumped VCSELs have additional loss mechanisms, our simulations show that even higher intrinsic quality of the cavity is reachable by increasing the radial dimension of the prisms. Therefore,  $Q$  factors exceeding what has been required for experimentally realized electrically injected lasers at blue wavelengths should be achievable using vertical cavities based on the GaN prisms reported here.

In the future, arrays of electrically injected prism-based vertical lasers could be realized if the GaN prism is combined with the growth of QWs on the atomically flat top c-facet, which has been demonstrated for LEDs using similar structures,<sup>34</sup> and standard fabrication techniques such as laser lift-off or electrochemical etching for substrate removal to enable the deposition of the bottom DBR. Furthermore, the controlled growth and the well-defined prism facets enable the exploration of evanescent coupling between neighboring cavities to tailor the emission characteristics and high-speed dynamics.<sup>35–37</sup>

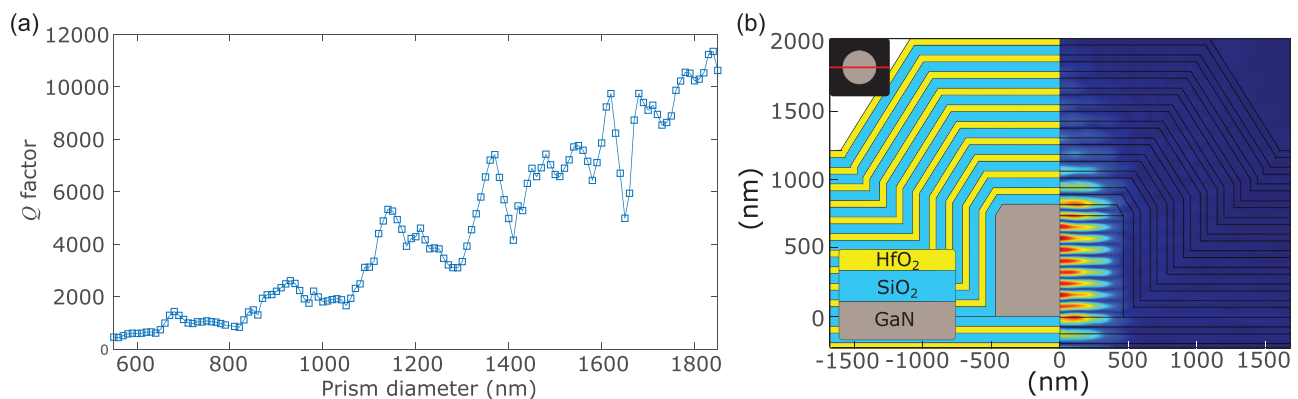


**FIG. 4.** (a)  $Q$  factors obtained by Q3D-FEM for GaN-prism cavities designed for resonance at a 420 nm wavelength and (b) the simulated circularly symmetric geometry (left half of the inset) and magnitude of the optical field in linear scale (right half) for a prism with a diameter of 940 nm. The red line in the inset marks the top-view direction of the cross section.

In conclusion, by using a nanowire-based and dislocation-free hexagonal GaN microprism as the central building block, we have demonstrated dislocation-free vertical microcavities with dielectric DBRs on both sides of the prism and investigated the importance of the prism width on the  $Q$  factor. The  $Q$  factor of the prism cavities increases with increasing width, and the measured  $Q$  factors for cavities with widths of 1000 nm are  $\sim 500$  in the yellow spectral regime, while only  $\sim 60$  for a cavity with a width of 600 nm. The measured  $Q$  values are in good agreement with those obtained from Q3D-FEM and 3D-BPM simulations. The simulations further predict  $Q$  factors of  $\sim 2000$  for the 1000 nm wide prism cavity in the targeted blue spectral regime, and such  $Q$  factors should be sufficient for prism-based vertical-cavity surface-emitting lasers. Thus, our results show that flat-top GaN microprisms can yield dislocation-free cavities with  $Q$  factors high enough for vertical-cavity lasers. These microcavities offer a starting-point for a small footprint laser with potential for low threshold current and long lifetime, with additional design freedom to tailor both emission properties and high-speed dynamics by coherent coupling between neighboring microcavities.

See the [supplementary material](#) for details on the GaN prism growth and the numerical simulation methods.

The authors would like to thank Saulius Marcinkevičius (Royal Institute of Technology, KTH) and Peder Bergman (Linköping University) for their valuable inputs on the optical measurements. This research was partly performed at the Lund Nano Lab. and the Chalmers Nanofabrication Lab., both facilities being part of the Myfab-network. The project was supported by the Swedish Research Council (VR), the Foundation for Strategic Research (SSF), the Knut and Alice Wallenberg foundation (KAW), the Swedish Energy Agency, Marie-Curie No. FP7-REA-GA 608153 (PhD4energy funding), and the Crafoord Foundation.

## DATA AVAILABILITY

The data that support the findings of this study are available from the corresponding author upon reasonable request.

## REFERENCES

- 1 J. Cho, J. H. Park, J. K. Kim, and E. F. Schubert, "White light-emitting diodes: History, progress, and future," *Laser Photonics Rev.* **11**, 1600147 (2017).
- 2 E. A. Jones, F. F. Wang, and D. Costinett, "Review of commercial GaN power devices and GaN-based converter design challenges," *IEEE J. Emerging Sel. Top. Power Electron.* **4**, 707–719 (2016).
- 3 Y. Nakatsu, Y. Nagao, T. Hirao, Y. Hara, S. Masui, T. Yanamoto, and S.-I. Nagahama, "Blue and green InGaN semiconductor lasers as light sources for displays," *Proc. SPIE* **11280**, 112800S (2020).
- 4 S. E. Bennett, "Dislocations and their reduction in GaN," *Mater. Sci. Technol.* **26**, 1017–1028 (2010).
- 5 Q. Dai, M. F. Schubert, M. H. Kim, J. K. Kim, E. F. Schubert, D. D. Koleske, M. H. Crawford, S. R. Lee, A. J. Fischer, G. Thaler, and M. A. Banas, "Internal quantum efficiency and nonradiative recombination coefficient of GaInN/GaN multiple quantum wells with different dislocation densities," *Appl. Phys. Lett.* **94**, 111109 (2009).
- 6 S. W. Kaun, M. H. Wong, S. Dasgupta, S. Choi, R. Chung, U. K. Mishra, and J. S. Speck, "Effects of threading dislocation density on the gate leakage of AlGaIn/GaN heterostructures for high electron mobility transistors," *Appl. Phys. Express* **4**, 024101 (2011).
- 7 P. Perlin, L. Marona, M. Leszczynski, T. Suski, P. Wisniewski, R. Czernecki, and I. Grzegory, "Degradation mechanisms of InGaN laser diodes," *Proc. IEEE* **98**, 1214–1219 (2010).
- 8 M. Kuramoto, S. Kobayashi, T. Akagi, K. Tazawa, K. Tanaka, T. Saito, and T. Takeuchi, "High-output-power and high-temperature operation of blue GaN-based vertical-cavity surface-emitting laser," *Appl. Phys. Express* **11**, 112101 (2018).
- 9 T. Hamaguchi, H. Nakajima, M. Tanaka, M. Ito, M. Ohara, T. Jyokawa, N. Kobayashi, T. Matou, K. Hayashi, H. Watanabe, R. Koda, and K. Yanashima, "Sub-milliamperethreshold continuous wave operation of GaN-based vertical-cavity surface-emitting laser with lateral optical confinement by curved mirror," *Appl. Phys. Express* **12**, 044004 (2019).
- 10 R. Colby, Z. Liang, I. H. Wildeson, D. A. Ewoldt, T. D. Sands, R. E. Garcia, and E. A. Stach, "Dislocation filtering in GaN nanostructures," *Nano Lett.* **10**, 1568–1573 (2010).
- 11 P.-M. Coulon, B. Alloing, V. Brändli, P. Vennéguès, M. Leroux, and J. Zúñiga-Pérez, "Dislocation filtering and polarity in the selective area growth of GaN nanowires by continuous-flow metal organic vapor phase epitaxy," *Appl. Phys. Express* **9**, 015502 (2016).
- 12 M. T. Björk, B. J. Ohlsson, T. Sass, A. I. Persson, C. Thelander, M. H. Magnusson, K. Deppert, L. R. Wallenberg, and L. Samuelson, "One-dimensional steeplechase for electrons realized," *Nano Lett.* **2**, 87–89 (2002).
- 13 E. P. A. M. Bakkers, J. A. van Dam, S. De Franceschi, L. P. Kouwenhoven, M. Kaiser, M. Verheijen, H. Wondergem, and P. van der Sluis, "Epitaxial growth of InP nanowires on germanium," *Nat. Mater.* **3**, 769–773 (2004).
- 14 K. L. Kavanagh, "Misfit dislocations in nanowire heterostructures," *Semicond. Sci. Technol.* **25**, 024006 (2010).
- 15 J. C. Johnson, H.-J. Choi, K. P. Knutsen, R. D. Schaller, P. Yang, and R. J. Saykally, "Single gallium nitride nanowire lasers," *Nat. Mater.* **1**, 106–110 (2002).
- 16 C. Li, J. B. Wright, S. Liu, P. Lu, J. J. Figiel, B. Leung, W. W. Chow, I. Brener, D. D. Koleske, T. S. Luk, D. F. Feezell, S. R. Brueck, and G. T. Wang, "Nonpolar InGaIn/GaN core-shell single nanowire lasers," *Nano Lett.* **17**, 1049–1055 (2017).
- 17 C. Y. Huang, J. J. Lin, T. C. Chang, C. Y. Liu, T. Y. Tai, K. B. Hong, T. C. Lu, and H. C. Kuo, "Collective lasing behavior of monolithic GaN-InGaIn core-shell nanorod lattice under room temperature," *Nano Lett.* **17**, 6228–6234 (2017).
- 18 K. H. Li, X. Liu, Q. Wang, S. Zhao, and Z. Mi, "Ultralow-threshold electrically injected AlGaIn nanowire ultraviolet lasers on Si operating at low temperature," *Nat. Nanotechnol.* **10**, 140–144 (2015).
- 19 Y.-H. Ra, R. T. Rashid, X. Liu, S. M. Sadaf, K. Mashooq, and Z. Mi, "An electrically pumped surface-emitting semiconductor green laser," *Sci. Adv.* **6**, eaav7523 (2020).
- 20 R. Chen, H. D. Sun, T. Wang, K. N. Hui, and H. W. Choi, "Optically pumped ultraviolet lasing from nitride nanopillars at room temperature," *Appl. Phys. Lett.* **96**, 241101 (2010).
- 21 A. Das, J. Heo, M. Jankowski, W. Guo, L. Zhang, H. Deng, and P. Bhattacharya, "Room temperature ultralow threshold GaN nanowire polariton laser," *Phys. Rev. Lett.* **107**, 066405 (2011).
- 22 J. Heo, S. Jahangir, B. Xiao, and P. Bhattacharya, "Room-temperature polariton lasing from GaN nanowire array clad by dielectric microcavity," *Nano Lett.* **13**, 2376–2380 (2013).
- 23 C. Tessarek, R. Röder, T. Michalsky, S. Geburt, H. Franke, R. Schmidt-Grund, M. Heilmann, B. Hoffmann, C. Ronning, M. Grundmann, and S. Christiansen, "Improving the optical properties of self-catalyzed GaN microrods toward whispering gallery mode lasing," *ACS Photonics* **1**, 990–997 (2014).
- 24 M. Behzadrad, M. Nami, N. Wostbrock, M. R. Zamani Kouhpanji, D. F. Feezell, S. R. J. Brueck, and T. Busani, "Scalable top-down approach tailored by interferometric lithography to achieve large-area single-mode GaN nanowire laser arrays on sapphire substrate," *ACS Nano* **12**, 2373–2380 (2018).
- 25 B. Damilano, P.-M. Coulon, S. Vézian, V. Brändli, J.-Y. Duboz, J. Massies, and P. A. Shields, "Top-down fabrication of GaN nano-laser arrays by displacement Talbot lithography and selective area sublimation," *Appl. Phys. Express* **12**, 045007 (2019).
- 26 Q. Sun, C. D. Yerino, B. Leung, J. Han, and M. E. Coltrin, "Understanding and controlling heteroepitaxy with the kinetic Wulff plot: A case study with GaN," *J. Appl. Phys.* **110**, 053517 (2011).
- 27 M. Khalilian, Z. Bi, J. Johansson, F. Lenrick, O. Hultin, J. Colvin, R. Timm, R. Wallenberg, J. Ohlsson, M.-E. Pistol, A. Gustafsson, and L. Samuelson,

- “Dislocation-free and atomically flat GaN hexagonal microprisms for device applications,” *Small* **16**, 1907364 (2020).
- <sup>28</sup>M. A. Reshchikov and H. Morkoç, “Luminescence properties of defects in GaN,” *J. Appl. Phys.* **97**, 061301 (2005).
- <sup>29</sup>A.-L. Henneghien, B. Gayral, Y. Désières, and J.-M. Gérard, “Simulation of waveguiding and emitting properties of semiconductor nanowires with hexagonal or circular sections,” *J. Opt. Soc. Am. B* **26**, 2396 (2009).
- <sup>30</sup>G. Lecamp, P. Lalanne, J. P. Hugonin, and J. M. Gérard, “Energy transfer through laterally confined Bragg mirrors and its impact on pillar microcavities,” *IEEE J. Quantum Electron.* **41**, 1323–1329 (2005).
- <sup>31</sup>S. Reitzenstein, N. Gregersen, C. Kistner, M. Strauss, C. Schneider, L. Pan, T. R. Nielsen, S. Höfling, J. Mørk, and A. Forchel, “Oscillatory variations in the Q factors of high quality micropillar cavities,” *Appl. Phys. Lett.* **94**, 061108 (2009).
- <sup>32</sup>T. Someya, R. Werner, A. Forchel, M. Catalano, R. Cingolani, and Y. Arakawa, “Room temperature lasing at blue wavelengths in gallium nitride microcavities,” *Science* **285**, 1905–1906 (1999).
- <sup>33</sup>T.-C. Lu, C.-C. Kao, H.-C. Kuo, G.-S. Huang, and S.-C. Wang, “CW lasing of current injection blue GaN-based vertical cavity surface emitting laser,” *Appl. Phys. Lett.* **92**, 141102 (2008).
- <sup>34</sup>Z. Bi, F. Lenrick, J. Colvin, A. Gustafsson, O. Hultin, A. Nowzari, T. Lu, R. Wallenberg, R. Timm, A. Mikkelsen, B. J. Ohlsson, K. Storm, B. Monemar, and L. Samuelson, “InGaN platelets: Synthesis and applications toward green and red light-emitting diodes,” *Nano Lett.* **19**, 2832–2839 (2019).
- <sup>35</sup>M. Kuramoto, S. Kobayashi, K. Tazawa, K. Tanaka, T. Akagi, and T. Saito, “In-phase supermode operation in GaN-based vertical-cavity surface-emitting laser,” *Appl. Phys. Lett.* **115**, 041101 (2019).
- <sup>36</sup>D. F. Siriani and K. D. Choquette, “Electronically controlled two-dimensional steering of in-phase coherently coupled vertical-cavity laser arrays,” *IEEE Photonics Technol. Lett.* **23**, 167–169 (2011).
- <sup>37</sup>H. Dalir and F. Koyama, “29 GHz directly modulated 980 nm vertical-cavity surface emitting lasers with bow-tie shape transverse coupled cavity,” *Appl. Phys. Lett.* **103**, 091109 (2013).